

1 Revision 1:

2 **Experimental tests on achieving equilibrium in synthetic fluid**
3 **inclusions: results for scheelite, molybdenite and gold solubility at**
4 **800°C and 200 MPa**

5
6
7 Insa T. Derrey*¹, Moritz Albrecht¹, Evgeniya Dupliy¹, Roman E. Botcharnikov¹,
8 Ingo Horn¹, Malte Junge², Stefan Weyer¹ & François Holtz¹

9
10
11
12
13 ¹ = Institut für Mineralogie, Leibniz Universität Hannover, Callinstr. 3, 30167 Hannover,
14 Germany

15 ² = Bundesanstalt für Geowissenschaften und Rohstoffe (BGR), Stilleweg 2, 30655 Hannover,
16 Germany

17
18
19 * = corresponding author: i.derrey@mineralogie.uni-hannover.de

24

Abstract

25 Synthetic fluid inclusions formed in high P/high T experiments, which are subsequently analyzed
26 with LA-ICP-MS, enable us to collect thermodynamic data to constrain metal transport in
27 aqueous fluids as well as partitioning of metals between coexisting phases. The most essential
28 prerequisite for such studies is to ensure that equilibrium conditions between liquid and solid
29 phases are reached prior to the formation of synthetic fluid inclusions in the host mineral. Various
30 methods have been proposed by different authors to achieve this goal, but to this point our
31 knowledge on the best approach to synthesize equilibrated fluid inclusions under constrained
32 pressure, temperature and compositional (P, T and X) conditions remains poor. In addition,
33 information on the time needed to reach equilibrium metal concentrations in the fluid as well as
34 on the timing of the onset of fluid inclusion formation in the host mineral are scarce.
35 The latter has been tested in a series of time-dependent experiments at 800°C and 200 MPa using
36 scheelite (CaWO₄), molybdenite (MoS₂) and metallic gold as dissolving phases and using
37 different approaches to optimize the formation of equilibrated fluid inclusions. Both f_{O_2} and f_{S_2}
38 were fixed during all experiments using the Pyrite-Pyrrhotite-Magnetite buffer (PPM). As an
39 intermediate in-situ quenching of the sample charge plays an important role in the synthesis of
40 fluid inclusions, we further tested the efficiency of such an intermediate quench for re-opening
41 fluid inclusions formed at 600°C and 200 MPa. Our results reveal that fluid inclusions start
42 forming almost instantaneously and that equilibrium between fluid and solid phases occurs in the
43 timescale of less than two hours for molybdenite and gold up to ca. 10 hours for scheelite. The
44 best approach to synthesize equilibrated fluid inclusions at 800°C was obtained by using an
45 intermediate quench on a previously unfractured quartz host. Experiments at 600°C showed
46 similar results and illustrate that this should be the method of choice down to this temperature.
47 Below 600°C pre-treatment of the quartz host (HF etching and/or thermal fracturing) becomes

2

48 important to produce large enough fluid inclusions for the analyses via LA-ICP-MS and special
49 care must be taken to prevent premature entrapment of the fluid.
50 Fluids with 8 wt% NaCl in equilibrium with scheelite, molybdenite and gold at 800°C and 200
51 MPa have concentrations of ca. 9200 ppm W, 1300 ppm Mo and 300 ppm Au, respectively,
52 which is in good agreement with results from other studies or extrapolation from lower
53 temperatures. It can be concluded that the formation of synthetic fluid inclusions from an
54 equilibrated fluid is possible, but different experimental designs are required, depending on the
55 investigated temperature. In general, dissolution of solid phases seems to be much faster than
56 previously assumed, so that experimental run durations can be designed considerably shorter,
57 which is of great advantage when using fast-consuming mineral buffers.
58 Keywords: synthetic fluid inclusions, equilibrium, scheelite solubility in aqueous fluid,
59 molybdenite solubility in aqueous fluid, gold solubility in aqueous fluid

60

61

Introduction

62 Magmatic and hydrothermal fluids play a crucial role in the formation of ore deposits, as they are
63 the main transporting agents controlling mobilization and selective concentration of elements in
64 the Earth's crust and, among others, metals of economic interest. Fluids trapped as fluid
65 inclusions in magmatic and hydrothermal minerals provide direct insight into the genesis and
66 evolution of natural fluids at the conditions of mineral growth or fracture healing. The correct
67 reconstruction of natural conditions e.g., during ore formation, however, requires accurate and
68 systematic quantification of the evolution of the fluid composition as a function of major
69 parameters that control the properties of magmatic or hydrothermal systems. The main approach
70 applied for such quantifications at high pressure (P) and temperature (T) is the experimental

71 synthesis of fluid inclusions which was described in the pioneering studies of Roedder and Kopp
72 (1975), Shelton and Orville (1980) and Sterner and Bodnar (1984).

73 The development of laser ablation inductively coupled plasma mass spectrometry (LA-ICP-MS)
74 techniques greatly improved the output of fluid inclusion studies, providing accurate quantitative
75 analysis of major, but also trace and volatile element concentrations (Günther et al., 1998; Seo et
76 al., 2011). In recent years, synthesis of fluid inclusions and subsequent LA-ICP-MS analysis have
77 become the methods of choice in collecting thermodynamic data constraining metal transport in
78 aqueous fluids and partitioning of metals between coexisting phases (e.g., Berry et al., 2006;
79 Duc-Tin et al., 2007; Frank et al., 2011; Hack and Mavrogenes, 2006; Hanley et al., 2005;
80 Heinrich et al., 1999; Lerchbaumer and Audetat, 2009; Loucks and Mavrogenes, 1999; Simon et
81 al., 2006; Ulrich and Mavrogenes, 2008; Zajacz et al., 2010; Zhang et al., 2012).

82 One of the main challenges in such studies is to ensure that equilibrium conditions between liquid
83 and solid phases were reached prior to the formation of fluid inclusions in the host mineral. For
84 example, Hanley et al. (2005) stated that it was “impossible to demonstrate that brine-metal
85 equilibrium was reached before fluid entrapment” in their experiments. There are two major
86 kinetic factors influencing the entrapment of equilibrated fluid inclusions in experimental studies:
87 a) the time necessary for the system to reach equilibrium with respect to all phases and buffer
88 mineral assemblages (t_{equil}) and b) the time needed to heal cavities in the respective host minerals
89 (quartz in most studies) (t_{heal}). Obviously, t_{heal} must be longer than t_{equil} to synthesize fluid
90 inclusions representing equilibrium fluids.

91 Since healing of cracks and mineral growth can occur quite fast, various methods have been
92 suggested to ensure achievement of equilibrium before fluid entrapment by delaying healing of
93 the host mineral, by reopening previously healed cracks or by opening new cracks after a defined
94 period of time. For instance, in their solubility study of NaCl and KCl in aqueous fluid, Sterner et

95 al. (1988) delayed crack healing of quartz by cycling pressure between 200 and 600 MPa in the
96 first two hours of the experiment. With this technique, the compression and decompression of the
97 fluid would lead to a continuous in- and out flux of the fluid through the cracks due to changes in
98 fluid density, keeping the fluid in the cracks of the host mineral connected with the surrounding
99 fluid. Using this approach, Sterner et al. (1988) were able to trap fluid inclusions with
100 homogenous salt concentrations even at very high salinities. Subsequently it was proven that
101 pressure cycling of about 100 MPa in total is sufficient to prevent fast healing of the cracks (P.
102 Lecumberri-Sanchez, personal communication).

103 More recently, Li and Audetat (2009) developed a method to synthesize larger fluid inclusions
104 under unfavorable growth conditions (e.g., low temperatures), which also provides a different
105 method to constrain the time of system equilibration before onset of fluid entrapment using a
106 *rapid heat/rapid quench cold seal pressure vessel* (RH/RQ-CSPV; design described in Matthews
107 et al. (2003)). This method was used and tested by Zhang et al. (2012), when investigating the
108 solubility of molybdenite in hydrothermal fluids. In a first step, they produced primary fluid
109 inclusions by growing a new layer of quartz over an etched quartz piece. In a second step, some
110 of the primary inclusions were reopened applying an intermediate quench using a rapid quench
111 system (drop from 800°C to \pm room temperature), which leads to in-situ fracturing of the quartz
112 cylinder. Subsequently, the sample was replaced into the hot zone to trap secondary inclusions in
113 the reopened cavities. Zhang et al. (2012) claimed that refilled inclusions trapped after the
114 intermediate quench can be distinguished optically from primary inclusions by the intersection of
115 cracks. Consequently, they could focus subsequent analysis of fluid inclusions via LA-ICP-MS
116 on inclusions that formed after quenching and reheating. They noted that these fluid inclusions
117 showed compositions considerably more constant than fluid inclusions from experiments without
118 an intermediate quench.

119 A similar approach was used by Zajacz et al. (2010), who trapped two generations of synthetic
120 fluid inclusions in a) a pre-fractured and b) a non pre-treated quartz chip in the same capsule,
121 whereas the latter was only fractured in-situ by the intermediate quench (drop from 1000°C to ±
122 room temperature after 24 h). They observed that the compositions of fluid inclusions in the pre-
123 fractured and in the in-situ fractured quartz chips were usually identical within uncertainty, which
124 supports their conclusion that equilibrium had been achieved before healing of the fractures in the
125 pre-fractured chip.

126 To this point our knowledge on the best approach (among those described above) to synthesize
127 equilibrated fluid inclusions remains poor. It is also not clear, which method is most suitable for
128 certain P, T and X conditions. The pioneering studies applying an intermediate quench by (Zhang
129 et al., 2012) and Zajacz et al. (2010) were performed at 600-800°C and 1000°C respectively and
130 they differ in their outcomes concerning the ubiquitous need for an intermediate quench. Little is
131 known about the efficiency of in-situ quenching at lower temperatures prevailing in the
132 hydrothermal regime of ore deposits. In addition, kinetic studies to constrain the actual time
133 necessary to equilibrate the fluid (t_{equil}) and trap it in the host mineral (t_{heal}) are still required.

134 In a series of experiments conducted at 800°C, 200 MPa and constant fO_2 and fS_2 (buffered by
135 the assemblage Pyrite-Pyrrhotite-Magnetite: PPM) we tested the effects of quartz pre-treatment,
136 pressure cycling and intermediate quenching on the formation and composition of metal-bearing
137 fluid inclusions which were trapped from aqueous fluids coexisting with molybdenite (MoS_2),
138 scheelite ($CaWO_4$) and gold at 800°C and 200MPa. To obtain a better understanding of the
139 relationship between t_{heal} and t_{equil} , we conducted a series of time-dependent experiments (1 to
140 100 hours). We further applied an experimental protocol to test the efficiency of an intermediate
141 quench and to distinguish fluid inclusions formed before and after an intermediate quench.

142 Finally, the results are used to discuss the solubility of molybdenite (MoS_2), scheelite (CaWO_4)
143 and metallic gold in aqueous fluids.

144

145

Experimental Procedure

146 All experiments were conducted in RH/RQ-CSPVs of the design described in Matthews et
147 al. (2003), using argon as pressure medium, at $T = 400\text{-}800^\circ\text{C}$ and $P = 200$ MPa.

148 Uncertainties of temperature and pressure measurements are considered to be $\leq \pm 5^\circ\text{C}$ and
149 ± 5 MPa, respectively. The external oxygen fugacity of our system was determined to be

150 ca. $\text{NNO}+2.3$ (i.e., 2.3 log units above the Ni-NiO buffer; Berndt et al., 2001). For

151 experiments using the PPM buffer, the phase assemblage after the run was analyzed by X-

152 ray diffractometry to check if all the buffer minerals were still present at the end of the

153 experiment, which they were in all cases. The capsule preparation for fluid inclusion

154 synthesis generally followed the workflow described by Bodnar et al. (1985) with some

155 modifications, which will be described below. Cylinders of 2.5 mm in diameter and ca. 2

156 mm in length were drilled out of inclusion-free alpine quartz. The cylinders were cleaned

157 in concentrated HCl for 30 minutes and in an ultrasonic bath with distilled water for 5

158 minutes. After specific pre-treatments, described below and in Fig. 1, quartz cylinders

159 were placed in Au capsules of ca. 25 mm length, 3.2 mm outer diameter and a wall

160 thickness of 0.2 mm together with an 8 wt% NaCl-solution, different mineral powders,

161 and silicagel to accelerate crack healing (for details see setup descriptions). The 8 wt%

162 NaCl-solution was spiked with 398 ppm Rb and 400 ppm Cs (concentrations were

163 calculated by gravimetry and confirmed by ICP-MS) and was used as internal standard

164 during LA-ICP-MS analysis (see also method in Duc-Tin et al. (2007)).

165 Capsules were pressurized to 200 MPa at room T and rapidly moved to the preheated hot
166 zone of the autoclave using the rapid heat device of the CSPV. The heating of the capsules
167 to the target T occurred rapidly, within a few minutes, at isobaric conditions. In some
168 experiments, the gold capsule was quenched quickly during the experiment by pulling the
169 Au capsule from the hot end of the vertical autoclave to the water-cooled end to cause
170 cracks within the quartz cylinder as a result of thermal stress (e.g., Li and Audetat, 2009).
171 After this “intermediate quench” step of a few seconds, the capsule was moved back to the
172 hot zone of the furnace. After a desired runtime, the autoclave was pulled out of the
173 furnace and slowly cooled to room temperature (ca. 30°C/min in the temperature range
174 800 – 300°C) to avoid unnecessary cracking of the quartz chip. The capsules were
175 weighed to check for potential leaks during the run. The recovered quartz cylinders were
176 cleaned, dried and embedded in araldite to be cut and polished to chips of ca. 300 µm
177 thickness.

178

179 **Setup 1: Experimental approach for equilibration tests at 800°C**

180 To identify the most reliable technique to synthesize fluid inclusions equilibrated with metal-
181 bearing phases, we compared the methods of Sterner et al. (1988), Zhang et al. (2012) and Zajacz
182 et al. (2010) that were described above. Each test was conducted in a Au capsule containing
183 molybdenite (MoS₂) and scheelite (CaWO₄) as a metal sources.

184 - *Experiment A:* For pressure cycling experiments, we used quartz cylinders that were
185 previously heated to 350°C in a muffle type furnace, quenched in distilled water, dried and
186 immersed in concentrated (40 wt%) hydrofluoric acid (HF) for 10 minutes to widen the
187 cracks. According to the design in Fig. 1a, one quartz cylinder was placed in a Au capsule
188 together with 25 µl of NaCl solution, 5-15 mg of each mineral powder, ca. 50 mg PPM

189 buffer (mixed in weight ratio 1 Pyrite : 3 Pyrrhotite : 1 Magnetite) and 3-5 mg of silicagel
190 powder.

191 - *Experiment B*: Capsules for experiments with the design of (Zhang et al., 2012) were
192 prepared in the same way, but quartz cylinders were not cracked thermally and only
193 immersed in concentrated HF for 30 minutes to produce cavities along the rim of the quartz
194 cylinder (Fig. 1b).

195 - *Experiment C*: Capsules that were designed according to Zajacz et al. (2010) contained two
196 quartz cylinders on top of each other (Fig. 1c), one was pre-treated in the same way as in
197 *Experiment A (C_1)* and one was not pre-treated, except for HCl cleaning in an ultrasonic
198 bath (*C_2*).

199 *Experiment A* was started as described above. Once the sample was moved into the hot zone,
200 which was pre-heated to 800°C, pressure (which was previously set to 200 MPa) was cycled from
201 150 MPa to 250 MPa for five times every 10 minutes for a total time span of 8 hours. After
202 pressure cycling, pressure was held constant at 200 MPa for three days before the capsule was
203 quenched slowly.

204 For *experiments B and C*, the capsules were moved into the hot zone of the pre-heated (800°C)
205 and pre-pressurized (200 MPa) autoclave. After two days at constant P and T, an intermediate
206 quench was conducted for approximately 10 seconds. The capsules were then left in the hot zone
207 for another three days before quenching slowly.

208

209 **Setup 2: Experimental approach to test the efficiency of an intermediate quench for re-** 210 **opening of fluid inclusions formed at 600°C**

211 In this approach, we tested to which extent the application of an intermediate quench is
212 successful for re-opening fluid inclusions. In the first phase of the experiment, the temperature

213 was fixed to 600°C (200 MPa). After the intermediate quench, temperature was set to 400°C
214 before the capsule was reentered into the hot zone. In this way, we were able to distinguish easily
215 between fluid inclusions formed before (600°C) and after the intermediate quench (400°C) via
216 microthermometry. To investigate the possible influence of different quartz pre-treatment each
217 experiment was performed with two capsules: one containing a quartz cylinder pre-treated as in
218 *experiment A* (cracked at 350°C plus 10 min in HF) and one containing quartz pre-treated in the
219 traditional way described by Sterner and Bodnar (1984), who only cracked the quartz thermally at
220 350°C. With the two different types of pre-treated quartz cylinders, a series of 2 x 3 Au-capsules
221 were prepared containing 2.5, 5 and 10 wt% NaCl solution and 2-6 mg silicagel powder. After 7
222 days at 600°C, the samples were quenched rapidly and left in the cold zone of the autoclave until
223 the furnace had cooled nearly isobarically to 400°C. The samples were then placed back into the
224 hot end of the autoclave, where they were left for 13 days at 400°C before the experiment was
225 terminated with a slow quench.

226

227 **Setup 3: Dissolution kinetics and time dependent experiments**

228 To assess the time necessary to form inclusions in pre-cracked quartz and to equilibrate
229 molybdenite, scheelite and gold with fluids at 800°C, we designed a series of experiments at 200
230 MPa with runtimes ranging from 1.8 to 100 hours. For each investigated run duration two gold
231 capsules were prepared, one containing molybdenite and the other one containing scheelite as
232 mineral powder. The capsule design was such that one quartz cylinder (pre-treated as in
233 *experiment A*: thermally cracked at 350°C plus 10 min in concentrated HF) was placed in a Au
234 capsule together with 25 µl of NaCl solution, 5-15 mg of the respective mineral powder, ca. 50
235 mg PPM buffer and 3-5 mg of silicagel powder. Experiments were run as described above
236 without an intermediate quench and the results compared to experiments from Setup 1.

237 Accounting for the exponential character of dissolution processes, the different runtimes were
238 chosen to be evenly distributed when plotted logarithmically.

239

240

Analytical Procedure

241 Fluid inclusions recovered from equilibration test and time dependent runs were analyzed for
242 their major and trace element contents by LA-ICP-MS. We applied a technique which is based on
243 the combination of a UV-femtosecond-laser (*Spectra Physics*) with a heating-freezing cell and a
244 high-resolution magnetic sector-field ICP-MS (*Element XR, Thermo Scientific*) (for details see
245 Albrecht et al., 2014). The in-house build laser ablation system is operating in the deep UV range
246 at 194 nm. A slightly modified INSTECTM heating-freezing stage with an adjusted cell volume of
247 3 cm³ is used as laser cell. Helium mixed with 2 vol% hydrogen (to adjust the hydrogen flow rate
248 to ca. 5-6 ml/min as suggested by Guillong and Heinrich (2007)) was used as sample-chamber
249 gas and mixed with argon downstream. Analyses were performed at temperatures of -60°C,
250 guaranteeing completely frozen fluid inclusions prior to the ablation, which resulted in an
251 excellent control on the opening of the inclusions and considerably longer signal analysis time.
252 The analytical uncertainty of the method is considered to be 10-30% for most elements as
253 described by Albrecht et al. (2014). NIST SRM 610 glass was used as external standard (using
254 reference values of the GeoReM database (Jochum et al., 2005)) and measured with a repetition
255 rate of 10 Hz after every fourth inclusion. Laser repetition rates for fluid inclusion analyses have
256 been 5 – 10 Hz, depending on the depth of the inclusion, with higher rates for deeper (up to 50
257 µm) inclusions. To evaluate the acquired data, the SILLS data reduction software (Guillong et al.,
258 2008) was used, which is particularly suitable for the interpretation of fluid inclusion signals. The
259 known Cs concentration of the starting fluid was used for internal standardization and compared
260 to Rb and Na concentrations, which were also known. Fluid inclusion analyses in which the

261 Rb/Cs-ratio deviated by more than 10% and/or the Na/Cs-ratio by more than 20% were discarded
262 as they are considered to represent analyses of poor quality (Zhang et al., 2012). Figure 2 shows a
263 representative spectrum of a fluid inclusion analysis.

264 Fluid inclusions from experiments testing the efficiency of an intermediate quench were
265 examined by microthermometry using a *Linkam FTIR600* heating-freezing stage. About 30 fluid
266 inclusions were analyzed from each quartz chip. Final ice melting temperatures (T_m) were
267 determined to check, if the resulting salinities corresponded to the weight salinities of the
268 different starting fluids. Homogenization temperatures (T_{hom}) were determined to distinguish
269 between fluid inclusions that formed prior to (600°C, 200 MPa) and after (400°C, 200 MPa) the
270 intermediate quench. The expected T_{hom} were calculated using the SoWat code, which comprises
271 the data of Driesner (2007) and Driesner and Heinrich (2007).

272

273 **Results**

274

275 **Setup 1: Equilibration tests**

276 All experimental run products from setup 1 contain abundant synthetic fluid inclusions varying in
277 size from a few μm to more than 100 μm (e.g. Fig. 3). Whereas the experimental designs *B* and
278 *C_1* produced a large amount of fluid inclusions with many of them in the preferable range for
279 LA-ICP-MS ($>10 \mu\text{m}$), designs *A* and *C_2* show on average smaller and less fluid inclusions, but
280 still abundant and large enough for analysis. Quartz chips made from cylinders from design *A*
281 (pressure cycling) deviate from the usually rectangular shape after the experiments (Fig. 4).

282 The outcome of the different experimental designs to achieve equilibrium between solid phases
283 and fluid are shown in Figure 5 and average values including standard deviations summarized in
284 Table 1. Metal concentrations in fluids from all experimental designs are in the same range

285 within error and correspond to approximately 6000 ppm W for scheelite-bearing samples, 1300
286 ppm Mo for molybdenite-bearing samples and 300 ppm Au, clustering within a standard
287 deviation range of ca. 10 – 25% (cf. Tab. 1). The pressure cycling experiment (design A),
288 however, resulted in fluid inclusions with a larger range in the analyzed concentrations (at least
289 for W and Au).

290

291 **Setup 2: Role of the intermediate quench**

292 Fluid inclusions in quartz cylinders, which were not only cracked at 350°C but additionally
293 etched in concentrated HF are considerably larger (many inclusions > 20 µm; Fig. 3b) than those
294 from cracked cylinders without etching (usually < 20 µm, mostly < 10 µm; Fig. 3a). Furthermore,
295 no fluid inclusions that formed at 400°C were measurable in the latter cylinders. Inclusions that
296 formed in cracked and etched quartz cylinders show clearly two distinct groups with different
297 T_{hom} , which can be related (after pressure correction according to Driesner and Heinrich (2007))
298 to the two different formation temperatures of 600°C and 400°C (Fig. 6, Table 2). Both
299 generations could be distinguished easily by their different T_{hom} via microthermometry, but it was
300 not possible to distinguish the two generations optically, which is in contrast to the observation
301 Zhang et al. (2012), who used an identical temperature of 800°C prior and after the intermediate
302 quench. Fluid inclusions that formed at 600°C and 400°C could not be distinguished according to
303 their distribution in the quartz chip, as they occur adjacent to each other in all parts of the quartz
304 (from center to rim) with no obvious relation to certain areas or surfaces.

305

306 **Setup 3: Time dependent experiments**

307 Figure 7 depicts the results of the time dependent experiments (summarized in Table 3). Even in
308 the two shortest runs (1.8 h and 3.2 h) abundant fluid inclusions were trapped in the quartz

309 crystals, but they are considerably smaller (mostly < 10 μm , few inclusion between 10 – 20 μm)
310 than those from longer runs, resulting in larger analytical errors due to insufficient counting
311 statistics. In this experimental series, no intermediate quench was performed, so that the large
312 range in concentrations of one element in fluid inclusions within one sample is primarily
313 interpreted to represent true variations due to different times of entrapment rather than analytical
314 error. Fluid inclusions which formed early in the experiment are expected to show non-
315 equilibrated metal concentrations.

316 Figure 7 demonstrates that the highest Mo and Au concentrations are in the same range in all
317 experiments (except for the shortest run where Mo concentrations are higher), independent
318 on the run duration. This indicates that equilibration of fluids with molybdenite and gold is fast
319 and reached within the first few hours of the experiment. On the other hand, the maximum W
320 concentrations increase within the first hours and remain constant after approximately 10 hours.

321

322 **Discussion**

323 In the following the outcome of the experiments are used to discuss the best approach for the
324 synthesis of equilibrated fluid inclusions.

325

326 **Size and number of fluid inclusions**

327 When preparing mineral cylinders to trap hydrothermal fluids during an experiment, we suggest a
328 pre-treatment of cylinders by both thermal cracking (10 min. at 350°C followed by quench in
329 room temperature distilled water) and immersion in concentrated HF for 10 minutes. If quartz is
330 pre-treated in this way, the formation of the highest number of fluid inclusions (compared to pre-
331 treatment with HF only) is observed and fluid inclusions have a considerably larger size
332 (compared to quartz that was only thermally cracked). This becomes especially important in

333 experiments at lower temperatures because fluid inclusions are usually too small for LA-ICP-MS
334 (ca. $< 10 \mu\text{m}$) or even microthermometry (ca. $< 5 \mu\text{m}$) under these conditions. Furthermore, our
335 experiments from setup 1 showed that fluid inclusions in both thermally cracked and HF-etched
336 quartz are more prone to in-situ fracturing by an intermediate quench, which becomes especially
337 important in experiments with long equilibration times.

338

339 **Dissolution kinetics**

340 From our time dependent experimental series (setup 3) for the dissolution of molybdenite,
341 scheelite and gold we gained two main insights, which are: 1) that fluid inclusions start to form
342 almost instantaneously ($< 1.8 \text{ h}$) under the applied conditions and 2) that the dissolution of the
343 investigated metal-bearing phases at 800°C is fast. As the metal concentrations from setup 3 are
344 very similar to those from setup 1 (equilibration tests; cf. Fig. 5 and 7), it can be concluded that
345 equilibrium of the fluid was reached in the time scale of a few hours ($< 1.8 \text{ h}$ to ca. 10 h). Thus,
346 although the fast formation of inclusions at 800°C has a negative influence on the formation of
347 equilibrated fluid inclusions, this effect is reduced by the fact that metal dissolution is
348 comparably fast. The fast entrapment of fluid inclusions in quartz emphasizes the importance of a
349 rapid heating autoclave, which keeps the time until the experimental temperature in the capsule is
350 reached at a minimum.

351 It is known that quartz solubility depends on the salinity of the fluid (e.g., Akinfiev and Diamond,
352 2009; Newton and Manning, 2000), which might possibly influence the velocity of crack healing.
353 Our time dependent series was conducted with an 8 wt% NaCl fluid. According to Newton and
354 Manning (2000) at this salinity and our experimental P/T conditions (800°C , 200 MPa) quartz
355 solubility is close to its maximum. Thus, any deviation in the salinity of the fluid would lead to a

356 decrease in quartz solubility. So if there was an effect it would likely be a delay of crack healing,
357 which would be advantageous for reaching equilibrium prior to entrapment of the fluid.

358 Whereas molybdenite and gold appear to dissolve and equilibrate very fast (faster than our
359 shortest experiment, with an apparent oversaturation of molybdenite in the shortest run),
360 maximum W concentrations from scheelite dissolution rise from ca. 2400 ppm after 1.8 h to ca.
361 7400 ppm within the first 10 hours, before they remain constant (Fig. 7). This might be due to the
362 more covalent bonding of W in the tungstate molecule and concomitant slower dissolution
363 kinetics compared to Mo from molybdenite and Au from native gold. Additionally, the different
364 crystal structure and chemical composition of scheelite, including Ca as an additional cation,
365 likely influences dissolution kinetics. Fast equilibration of Au concentration was also shown by
366 Benning and Seward (1996), who determined Au equilibration times of roughly 3 days at 150°C,
367 1.5 days at 200°C, 1 day at 300°C and “a few hours” at 500°C. Exponential extrapolation of this
368 dataset results in an equilibration time of <1 h at 800°C, which is in perfect agreement with our
369 findings.

370 Our results indicate that time dependent series similar to ours are useful to get an estimate of
371 optimal run durations needed to equilibrate the system of interest with respect to all phases
372 including buffers. Findings of Zajacz et al. (2010) showed that there are cases where equilibration
373 might take longer, e.g. due to a slowly adjusting buffer. In their experiments, this occurred in a
374 case study where a large amount of H₂ had to diffuse out of the gold capsule to achieve redox
375 equilibrium and crack healing was apparently faster than the time needed to equilibrate the
376 system. As a result, the compositions of fluid inclusions were different in a pre-treated and in a
377 previously unfractured and in-situ quenched quartz chip. However, in most systems metal
378 concentrations seem to equilibrate fast enough to be studied by synthetic fluid inclusion
379 technique, which is also supported by the findings of Simon et al. (2007). According to them,

380 quartz crack healing is slow enough to allow the entrapment of fully equilibrated fluids at 800°C
381 and 100 MPa in the haplogranite – magnetite – gold – NaCl – KCl – HCl – H₂O system, but no
382 estimate of crack healing times is given. Simon et al. (2007) further highlighted the importance of
383 a low thermal gradient ($\leq\pm 5^\circ\text{C}$) across the experimental charge to prevent the formation of a
384 rapidly precipitating primary quartz overgrowth. We determined a temperature gradient of $\leq\pm 2^\circ\text{C}$
385 over the length of 3 cm for our experimental charges.

386

387 **Importance of intermediate quench**

388 As shown by Zhang et al. (2012), Zajacz et al. (2010) and this study, an intermediate quench (i.e.,
389 in-situ quartz cracking) after a long enough equilibration time will lead to the smallest scatter in
390 metal concentrations from the resultant fluid inclusions. In our equilibration tests at 800°C, the
391 best results were achieved with fluid inclusions formed after an intermediate quench in quartz
392 cylinders which were not pre-treated (Fig. 5, design C_2). This could be expected, as this
393 approach is the only design in which inclusions cannot form before the intermediate quench (we
394 did not observe formation of quartz overgrowth which could have led to entrapment of primary
395 fluid inclusions). The drawback of this method is that it gets increasingly less effective at lower
396 temperatures. Thus, the design C_2 is appropriate and recommended for experiments at rather
397 high temperatures (1000°C, Zajacz et al. (2010); 800°C, this study).

398 From our experience, it was only possible to induce enough cracks in quartz and to produce fluid
399 inclusions sufficiently large for LA-ICP-MS by an intermediate quench down to a temperature of
400 ca. 600°C. Below 600°C only few and very small inclusions form in the unfractured quartz and
401 such inclusions were not suitable for LA-ICP-MS. Figure 3 c) and d) show the different
402 appearance of fluid inclusions formed in an unfractured quartz chip by an intermediate quench at
403 800°C and 600°C, respectively. Both, the abundance and size of synthetic fluid inclusions

404 decrease rapidly with decreasing temperature. Thermal cracking is further hindered by the use of
405 double capsules (Eugster, 1957 and following), which makes in-situ cracking less effective than
406 in single capsules. Therefore, in-situ cracking of initially unfractured quartz by an intermediate
407 quench should be the method of choice for synthesis of fluid inclusions at high temperatures, but
408 it is less useful at temperatures below 600°C. In any case, it is recommendable to add a pre-
409 treated quartz (of design *B* or *C_1*) to the capsule to ensure the formation of sufficient fluid
410 inclusions of optimal size, which can then be compared to inclusions from initially unfractured
411 quartz. In our experiments, the results from design *B* and *C_1* show only minor deviation from
412 results of design *C_2* with not pre-treated, in-situ cracked quartz, but a larger range in the
413 individual analyses (Fig. 5). However, both designs are recommended for experiments below
414 600°C, as they will ensure the formation of adequate fluid inclusions down to at least 400°C. Our
415 experiments testing the re-opening of fluid inclusions after an intermediate quench showed that
416 in-situ quenching and subsequent formation of new fluid inclusions works down to at least 600°C
417 (Fig. 6B). The replacement of fluid inclusions, however, only occurs partly and we were not able
418 to distinguish optically between fluid inclusions that formed prior to and after the intermediate
419 quench. Thus, the interpretation of LA-ICP-MS of fluid inclusions that formed after the
420 intermediate quench may be difficult. The yield of equilibrated fluid inclusions might be
421 increased by quenching the sample in-situ several times in short succession (R. Linnen, personal
422 communication).

423

424 **Limitations of pressure cycling**

425 Equilibration design *A* (pressure cycling) does not seem suitable for our conditions, as the metal
426 concentrations in fluid inclusions show the largest range in concentrations (but comparable
427 values in average, Fig. 5). This is interpreted to be due to several factors. One possible reason

428 could be that the duration of pressure cycling (8 hours) was too short for the metal concentrations
429 to equilibrate. But this interpretation is not confirmed by the results from the time dependent
430 experiments, at least for Mo and Au (Fig. 7). A second possible explanation is that some
431 inclusions with low metal concentrations formed in the very early stages of the experiment and
432 were not re-opened despite of pressure cycling. Possibly, a higher total pressure difference is
433 needed after all (as applied by Sterner et al. (1988)) to change the fluid density enough to prevent
434 the cracks from healing. Yet another explanation would be that some inclusions decrepitated as a
435 result of pressure variation, which may explain anomalous high and low metal concentrations.
436 The observed change in shape of the quartz cylinders after the experiment (Fig. 4) might be due
437 to deformation of the quartz during the experiment, which may indicate that partial decrepitation
438 occurred during pressure cycling. This would imply that a temperature of 800°C is too high for
439 pressure cycling experiments, as the quartz crystal becomes ductile and deforms in response to
440 the oscillating pressure. However, no decrepitation of fluid inclusions was observed under the
441 microscope and the observed change in shape could also be the result of quartz overgrowth along
442 preferred crystallographic orientations. Fluctuations in quartz solubility during pressure cycling
443 may have resulted in enhanced dissolution and reprecipitation of quartz. At lower temperatures
444 this effect should also be minimized so that, with an appropriate cycling period and pressure
445 difference, this method might be the method of choice for some applications at low temperatures,
446 as e.g., described by Sterner et al. (1988). The use of a different host mineral, which is less
447 soluble than quartz at high temperatures, could possibly expand the applicability of this method
448 to higher temperatures.

449

450 **Au, Mo and W concentrations in fluids in equilibrium with Au metal, molybdenite and**
451 **scheelite**

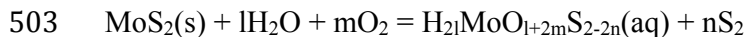
452 As Au and Mo concentrations in fluid inclusions from all experimental designs are identical
453 within error (except for the shortest run from setup 3, where Mo concentrations are higher)
454 and are in the same range as the maximum concentrations determined in the time dependent
455 experiments, they are interpreted to represent concentrations in 8 wt% NaCl fluids in equilibrium
456 with Au metal and molybdenite at 800°C, 200 MPa and PPM buffered conditions. Comparing
457 maximum W concentrations from the equilibration tests and time dependent experiments, it is
458 noticeable that W concentrations are slightly lower in the former (ca. 6100 ppm versus ca. 7400
459 ppm). This might be a result of the relatively large scatter of W concentrations (standard
460 deviation ca. 2000 ppm) in the time dependent experiments, which were performed without an
461 intermediate quench. However, the difference in the capsule design between the two setups is that
462 in the equilibration tests scheelite and molybdenite were placed together in the same capsule,
463 whereas capsules with either scheelite or molybdenite were prepared for the time dependent
464 experiments. Therefore, W solubility could be dependent on Mo in the system, whereas Mo
465 concentrations do not change notably between both experimental designs and are in the order of
466 1300 ppm, which is also in good agreement with the data from Zhang et al. (2012, see *2 in Fig.
467 5), who performed experiments with molybdenite only and who reported average Mo
468 concentrations for experiments of the same design of 1200 to 1510 ppm. This may indicate that
469 W and Mo, both of which are hard Lewis acids, compete for the same ligands (e.g., OH⁻, O²⁻, Cl⁻)
470 but that Mo forms the more stable complexes and is thus complexed preferentially, possibly due
471 to the slightly higher difference in electronegativity with respect to oxygen.

472 Figure 5 (*1) also shows W concentration extrapolated from scheelite solubility data from Foster
473 (1977) obtained between 252 and 529°C in the pressure range 100-200MPa. Assuming a linear
474 correlation of logW(ppm) vs. 1000/(T in K), a least square extrapolation resulted in a value of ca.
475 1200 ppm (or 1900 ppm if two obvious outliers are discarded). This is lower by a factor of ~ 3-5

476 when compared to our data (fluids in equilibrium with scheelite only) and the possible variation
477 may be due to the use of a different buffer (Msk-Kfs-Qz) and salt in the solution (1 M KCl,
478 which corresponds to 7.17 wt% KCl), but likely also due to quenching problems and the
479 formation of precipitates, as Foster (1977) sampled the fluid directly from the capsule. Loucks
480 and Mavrogenes (1999), who applied the synthetic fluid inclusion approach investigated the
481 solubility of gold. Extrapolation of their Au concentrations from experiments in the range of 625
482 to 725°C led to a value of roughly 220 ppm Au (Fig. 5, *3), which is slightly lower than our
483 results of ca. 300 ppm. Even though their experiments were performed under the same buffer
484 conditions (PPM), other experimental conditions differed, which may explain the small
485 discrepancy. In particular, the experiments were conducted at 110 MPa and they used a 1 m HCl
486 solution. Extrapolation of Au concentrations determined via direct fluid sampling from the
487 capsule by Gibert et al. (1998) in the range of 350 to 450°C leads to a value of roughly 40 ppm
488 Au, which is considerably lower than our results. The experiments of Gibert et al. (1998) were
489 performed under the same buffer conditions (PPM), but were conducted at 50 MPa and the
490 authors additionally used the Msk-Kfs-Qz buffer and a 0.5 M KCl solution. The lower
491 concentration might also stem from quenching problems and the formation of quench
492 precipitates. In general, extrapolation to higher temperatures and pressures must be applied with
493 caution, as metal complexation at low P-T conditions may be different from that at higher P-T
494 (Pokrovski et al., 2015).

495 It was previously mentioned that analyses from the shortest time dependent experiment are
496 subject to a large analytical error due to the small size of produced fluid inclusions. Therefore,
497 the slightly higher Mo concentrations in the experiment compared to the longer durations might
498 be solely explained by bad counting statistics. It cannot be ruled out though that Mo experiences
499 a true early oversaturation, which might be due to a lower fS_2 in the fluid before the Pyrite-

500 Pyrrhotite-Magnetite buffer has equilibrated. Following Chatelier's principle a lower fS_2 would
501 lead to a distortion of the dissolution equilibrium as proposed by Zhang et al. (2012) in favor of
502 the side with the dissolved species:



504

505

Implications

506 In this study we confirmed that synthetic fluid inclusions are a successful tool to probe fluids in
507 experiments at high temperatures and pressures without the problem of fluid quenching.
508 Solubilities of solid phases in different fluids can be determined under various conditions,
509 including the possibility to access partitioning data of elements between various phases.
510 However, the implication of the discussion is that there is currently no universal and perfect
511 experimental design for the synthesis of equilibrated fluid inclusions. Depending on the
512 investigated temperature, pressure, equilibrating phases and host mineral in the experiments,
513 different designs need to be applied to obtain reliable result.

514 For experiments with $T \geq 600^\circ\text{C}$, we recommend the use of our experimental design C, as from
515 our experience this design produces results of the best quality. In particular, applying an
516 intermediate quench (or possibly several) after a well-defined equilibration time is strongly
517 recommended. Time dependent experiments showed that mineral dissolution is considerably
518 faster than usually assumed (e.g. Hanley et al., 2005; Simon et al., 2007; Zhang et al., 2012). The
519 dissolution of scheelite takes slightly longer than that of molybdenite and gold, but is still in the
520 order of hours rather than days at 800°C . As a consequence, experimental durations can be
521 designed much shorter than previously done, which is a great advantage when using fast
522 consuming solid mineral buffers. Nevertheless, equilibration times of the used buffer also need to

523 be taken into account when deciding on the length of the experiment prior to the intermediate
524 quench.

525 For experiments distinctly below 600°C, the use of an unfractured additional mineral cylinder can
526 be discarded, as it does not yield fluid inclusions that are large enough for LA-ICP-MS analysis.

527 It is, however, possible to produce adequate fluid inclusions down to at least a temperature of
528 400°C in doubly pre-treated quartz cylinders. But care must be taken in estimating t_{heal} and t_{equil} ,

529 which will be longer than at higher temperatures. Below 400°C we were not able to produce fluid
530 inclusions which were suitable for LA-ICP-MS, so that different experimental approaches (e.g.,

531 direct sampling of the fluid in a reaction cell autoclave such as the design of Seyfried et al.
532 (1979)) need to be applied.

533

534

Acknowledgments

535 We thank Dionysis Foustoukos for editorial handling as well as two anonymous reviewers,
536 whose critical reviews of an earlier version significantly improved this manuscript. We

537 thank U. Kropp for his technical support as well as J. Feige for sample preparation. We are
538 grateful for helpful discussions with P. Lecumberri-Sanchez and R. Linnen. This work was

539 funded by the State of Lower Saxony (Germany), Graduate School GeoFluxes as well as the
540 Leibniz Universität Hannover.

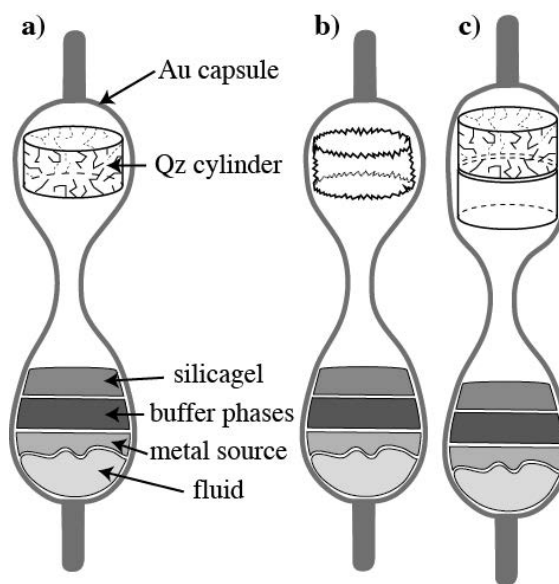
541

542

Figures

543 Figure 1: Different capsule designs: a) with quartz cylinder, which was pre-fractured at 350°C
544 and put into concentrated HF for 10 min, b) with quartz cylinder etched in concentrated HF for
545 30 min, c) with two quartz cylinders, one of which was pre-treated as in a) and the other was
546 cleaned in HCl only; note that all capsules were crimped in the center, so that the quartz
547 cylinder(s) were not in direct contact with the other phases of the experimental charge prior to the
548 experiment. All capsules contained aqueous fluid with different NaCl concentrations,
549 molybdenite and/or scheelite as Mo and W source respectively, silicagel to enhance quartz
550 heeling as well as the mineral assemblage Pyrite-Pyrrhotite-Magnetite to buffer fO_2 and fS_2 (PPM
551 buffer). Gold capsules served as a source for Au in the experiments.

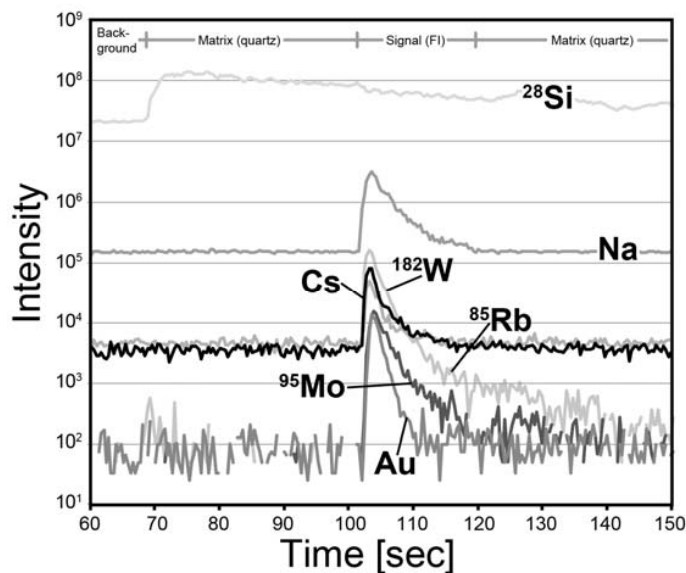
552



553

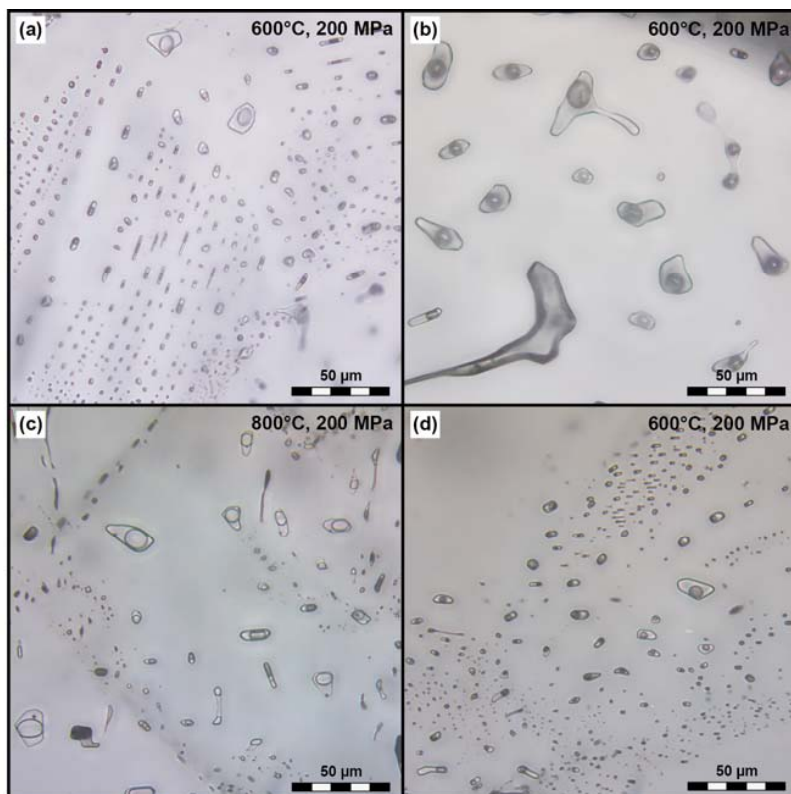
554

555 Figure 2: Typical LA-ICP-MS signal from a frozen fluid inclusion (metal source: molybdenite +
556 scheelite + gold, formed at 800°C, 200 MPa, PPM buffer) using a UV-fs-laser, heating-freezing
557 cell and *Element XR* ICP-MS.



558

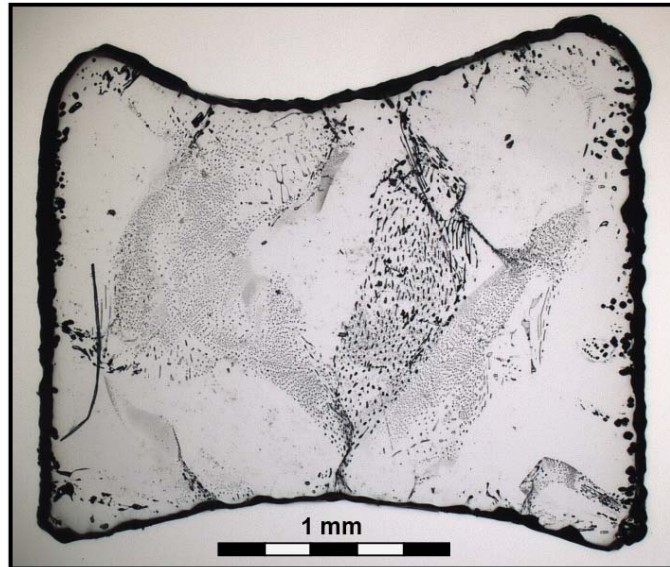
559 Figure 3: Typical appearance of synthetic fluid inclusions formed (a) at 600°C and 200 MPa in
560 quartz that was only pre-cracked at 350°C, (b) at 600°C and 200 MPa in quartz that was pre-
561 cracked at 350°C and immersed in concentrated HF for 10 minutes, (c, d) in-situ by an
562 intermediate quench in a previously unfractured quartz at (c) 800°C and (d) 600°C and 200MPa.
563



564

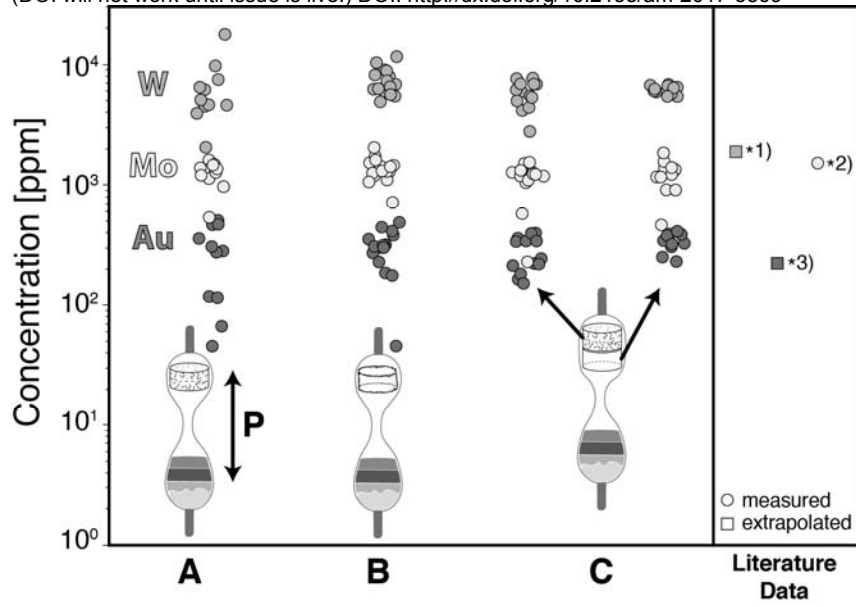
565 Figure 4: Polished section of quartz chip from pressure cycling *experiment A*. Note the convex
566 top and bottom faces of the cylinder, which were roughly parallel to each other prior to the
567 experiment.

568



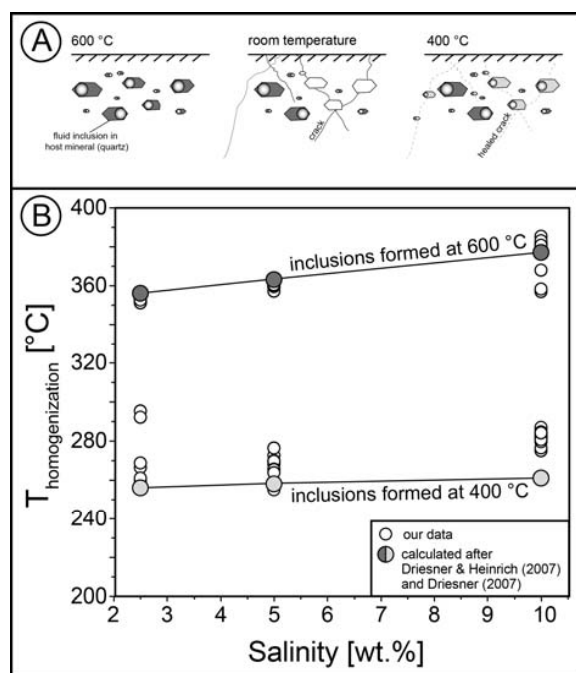
569

570 Figure 5: Results from setup 1 (equilibrations tests) using different approaches: Fluid
571 concentrations of W from scheelite dissolution, Mo from molybdenite dissolution and Au from
572 metallic gold dissolution at 800°C, 200 MPa and fO_2 and fS_2 conditions buffered by Pyrite-
573 Pyrrhotite-Magnetite (PPM). **Experiment A**: results from pressure cycling experiment (150 MPa
574 to 250 MPa for five times every 10 minutes for 8 hours, followed by 3 days at 200 MPa) with
575 pre-cracked (350°C to room temperature) and pre-etched (10 min in concentrated HF) quartz
576 cylinder, **Experiment B**: results from experiment with pre-etched (30 min in concentrated HF)
577 quartz cylinder and intermediate quench (2 + 3 days), **Experiment C**: results from experiment
578 with two quartz cylinders (left/top: pre-cracked and pre-etched (350°C to room temperature
579 followed by 10 min in concentrated HF), right/bottom: not pre-treated) and intermediate quench
580 (2 + 3 days), **Literature Data**: *1) W concentration extrapolated to 800°C using data from Foster
581 (1977, 252-529°C, 100-200 MPa, muscovite – K-feldspar – quartz buffer + 1 M KCl, metal
582 source was also scheelite), *2) measured Mo concentration from Zhang et al. (2012, 800°C, 200
583 MPa, PPM buffer, 8 wt% NaCl, metal source: molybdenite), *3) Au concentration extrapolated to
584 800°C using data from Loucks and Mavrogenes (1999, 625-725°C, 110 MPa, PPM buffer, 1 m
585 HCl, metal source: metallic gold).
586



587

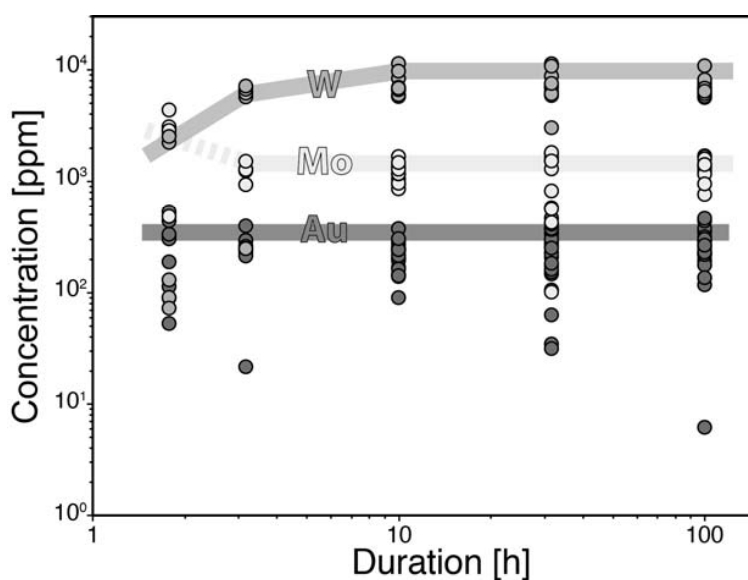
588 Figure 6: A) Strategy applied to test the role of intermediate quench on fluid inclusion formation
589 (setup 2). From left to right: 1. Formation of fluid inclusions in pre-treated (pre-cracked at 350°C
590 and immersed in concentrated HF for 10 minutes) quartz cylinder at 600°C (200 MPa) – 2.
591 Intermediate quench of the sample from 600°C to room temperature, leading to the formation of
592 new cracks and opening of some of the early formed fluid inclusions – 3. Formation of new and
593 refilled fluid inclusions at 400°C by healing of the newly formed cracks. B) Results from setup 2:
594 Measured homogenization temperatures (T_{hom}) of fluid inclusions in our three samples versus
595 fluid salinity (white circles). Grey circles depict calculated T_{hom} for 400°C (light grey) and 600°C
596 (dark grey) and 200 MPa for the different fluid salinities after Driesner and Heinrich (2007) and
597 Driesner (2007).
598



599

600 Figure 7: Results from setup 3 (time dependent experiments): concentrations of W from scheelite
601 dissolution (grey circles), Mo from molybdenite dissolution (light grey circles) and Au (dark grey
602 circles) from native gold dissolution after different runtimes (1.8 to 100 h) at 800°C, 200 MPa
603 and f_{O_2} and f_{S_2} conditions buffered by the PPM buffer. Transparent lines roughly trace the
604 development of maximum metal concentrations with time. See text for discussion of initially
605 higher Mo values (indicated by dashed line).

606



607

608

Tables

609 Table 1: Summary of experiments from setup 1 and respective results. W, Mo and Au
 610 concentrations are given in ppm by weight.

611

#	Type	T [°C]	P [MPa]	Composition	logfO ₂ [bar]	logfS ₂ [bar]	n	W [ppm] in fluid		Mo [ppm] in fluid		Au [ppm] in fluid	
								Avg	Stdev	Avg	Stdev	Avg	Stdev
A	P-cycling	800	200	8 wt% NaCl, Mol, Sch, PPM	-11.2	0.4	11	6370	4000	1320	180	270	160
B	HF pre-treatment	800	200	8 wt% NaCl, Mol, Sch, PPM	-11.2	0.4	16	7370	1740	1400	250	330	80
C_1	350°C + HF	800	200	8 wt% NaCl, Mol, Sch, PPM	-11.2	0.4	13	5900	1280	1260	140	280	90
C_2	not pre-treated	800	200	8 wt% NaCl, Mol, Sch, PPM	-11.2	0.4	12	6100	470	1290	270	330	60

612 n: number of analyzed fluid inclusions after discarding analysis with Cs/Rb and Na/Rb ratios deviating by more than 10 % and 20% of the initial
 613 fluid, respectively.

614 8 wt% NaCl, Mol, Sch, PPM: Fluid with 8 wt% NaCl coexisting with molybdenite, scheelite and PPM buffer

615 logfO₂, logfS₂: according to Zhang et al. (2012)

616 logfO₂ of -11.2 corresponds to NNO +2.5 at 800°C and 200 MPa

617 Table 2: Homogenization temperatures from pre-cracked and etched quartz cylinders from setup
 618 2. Experiments were run as described in the text at 200 MPa with three different salinities at
 619 600°C prior and 400°C after the intermediate quench. Calculated temperatures were obtained
 620 from the SoWat model of Driesner and Heinrich (2007) and Driesner (2007).

Sample	#	Salinity [wt% NaCl]	T _{hom} [°C]	Sample	#	Salinity [wt% NaCl]	T _{hom} [°C]	Sample	#	Salinity [wt% NaCl]	T _{hom} [°C]
ID 145	1	2.5	266	ID 146	1	5	273	ID 147	1	10	281
	2	2.5	351		2	5	360		2	10	385
	3	2.5	351		3	5	359		3	10	382
	4	2.5	352		4	5	359		4	10	382
	5	2.5	354		5	5	360		5	10	275
	6	2.5	269		6	5	361		6	10	276
	7	2.5	352		7	5	360		7	10	382
	8	2.5	351		8	5	270		8	10	382
	9	2.5	352		9	5	276		9	10	282
	10	2.5	352		10	5	359		10	10	284
	11	2.5	352		11	5	268		11	10	n.d.
	12	2.5	351		12	5	359		12	10	n.d.
	13	2.5	351		13	5	269		13	10	283
	14	2.5	351		14	5	359		14	10	283
	15	2.5	354		15	5	359		15	10	284
	16	2.5	353		16	5	360		16	10	282
	17	2.5	353		17	5	255		17	10	357
	18	2.5	353		18	5	269		18	10	358
	19	2.5	353		19	5	n.d.		19	10	281
	20	2.5	353		20	5	357		20	10	280
	21	2.5	260		21	5	362		21	10	281
	22	2.5	261		22	5	361		22	10	286
	23	2.5	355		23	5	359		23	10	287
	24	2.5	353		24	5	270		24	10	285
	25	2.5	n.d.		25	5	360		25	10	284
	26	2.5	295		26	5	360		26	10	368
	27	2.5	353		27	5	360		27	10	380
	28	2.5	292		28	5	266		28	10	380
	29	2.5	n.d.		29	5	265		29	10	383
	30	2.5	353		30	5	264		30	10	381
calculated (400°C, 200MPa)		2.5	256	calculated (400°C, 200MPa)		5	258	calculated (400°C, 200MPa)		10	261
calculated (600°C, 200MPa)		2.5	356	calculated (600°C, 200MPa)		5	364	calculated (600°C, 200MPa)		10	378

621

622

623 Table 3: Results from the time dependent series from setup 3. All experiments were run at 800
 624 °C, 200 MPa with an 8 wt% NaCl fluid and buffered by the PPM buffer. The sources for the
 625 metals were native gold of the capsule material and molybdenite or scheelite, respectively.

626

Duration [h]	Molybdenite Series			Scheelite Series		
	Sample	Mo [ppm]	Au [ppm]	Sample	W [ppm]	Au [ppm]
100	ID 191	1370	272	ID 192	5610	229
		1686	365		6175	220
		1419	347		5723	234
		1355	254		6377	221
		1317	262		6905	289
		754	6		7468	290
		1158	294		6620	300
		1652	377		10792	117
		1582	437		5758	176
		1231	193		8097	218
		1406	461		6061	229
		1157	223		6793	265
		1408	293		6382	136
		760	215			
945	315					
31.6	ID 194	1527	464	ID 193	6282	63
		1749	340		3007	280
		1515	300		8687	105
		1612	365		6968	333
		575	174		7374	bdl
		816	161		8710	146
		1288	221		5920	257
		562	182		11239	206
		1773	374		5847	153
		1805	408		6849	265
		101	bdl		6961	300
		424	31		6039	34
		1516	250		10707	229
					7492	380
10	ID 195	1660	240	ID 197	6537	270
		939	144		14755	90
		1336	290		8311	373
		bdl	bdl		5764	201
		1350	144		5726	162
		1049	168		6918	139
		853	250		5935	214
		958	201		6647	242
		1160	193		6587	251
		1166	243		6810	242
		1277	213		11308	141
		1468	233		9661	303

3.17	ID 196	1285	240	ID 198	6335	212
		1238	288		247	22
		931	239		5672	bdl
		1267	260		6135	293
		1506	395		6655	258
		930	226		7105	248
1.78	ID 200	4340	302	ID 199	2221	323
		2567	528		130	53
		3067	332		2512	438
		2840	188		90	113
		481	89		72	bdl

*bdl: below detection limit

627
628

References

- 630 Akinfiyev, N.N., and Diamond, L.W. (2009) A simple predictive model of quartz solubility in
631 water-salt-CO₂ systems at temperatures up to 1000 degrees C and pressures up to
632 1000 MPa. *Geochimica Et Cosmochimica Acta*, 73(6), 1597-1608.
- 633 Albrecht, M., Derrey, I.T., Horn, I., Schuth, S., and Weyer, S. (2014) Quantification of trace
634 element contents in frozen fluid inclusions by UV-fs-LA-ICP-MS analysis. *Journal of*
635 *Analytical Atomic Spectrometry*, 29(6), 1034-1041.
- 636 Benning, L.G., and Seward, T.M. (1996) Hydrosulphide complexing of Au(I) in hydrothermal
637 solutions from 150-400 degrees C and 500-1500bar. *Geochimica Et Cosmochimica*
638 *Acta*, 60(11), 1849-1871.
- 639 Berndt, J., Holtz, F., and Koepke, J. (2001) Experimental constraints on storage conditions in
640 the chemically zoned phonolitic magma chamber of the Laacher See volcano.
641 *Contributions to Mineralogy and Petrology*, 140(4), 469-486.
- 642 Berry, A.J., Hack, A.C., Mavrogenes, J.A., Newville, M., and Sutton, S.R. (2006) A XANES study
643 of Cu speciation in high-temperature brines using synthetic fluid inclusions.
644 *American Mineralogist*, 91(11-12), 1773-1782.
- 645 Driesner, T. (2007) The system H₂O-NaCl. Part II: Correlations for molar volume, enthalpy,
646 and isobaric heat capacity from 0 to 1000 degrees C, 1 to 5000 bar, and 0 to 1 X-
647 NaCl. *Geochimica Et Cosmochimica Acta*, 71(20), 4902-4919.
- 648 Driesner, T., and Heinrich, C.A. (2007) The system H₂O-NaCl. Part I: Correlation formulae
649 for phase relations in temperature-pressure-composition space from 0 to 1000
650 degrees C, 0 to 5000 bar, and 0 to 1 X-NaCl. *Geochimica Et Cosmochimica Acta*,
651 71(20), 4880-4901.
- 652 Duc-Tin, Q., Audetat, A., and Keppler, H. (2007) Solubility of tin in (Cl, F)-bearing aqueous
653 fluids at 700 degrees C, 140 MPa: A LA-ICP-MS study on synthetic fluid inclusions.
654 *Geochimica Et Cosmochimica Acta*, 71(13), 3323-3335.
- 655 Eugster, H.P. (1957) Heterogeneous Reactions Involving Oxidation and Reduction at High
656 Pressures and Temperatures. *Journal of Chemical Physics*, 26(6), 1760-1761.
- 657 Foster, R.P. (1977) Solubility of Scheelite in Hydrothermal Chloride Solutions. *Chemical*
658 *Geology*, 20(1), 27-43.
- 659 Frank, M.R., Simon, A.C., Pettke, T., Candela, P.A., and Piccoli, P.M. (2011) Gold and copper
660 partitioning in magmatic-hydrothermal systems at 800 degrees C and 100 MPa.
661 *Geochimica Et Cosmochimica Acta*, 75(9), 2470-2482.
- 662 Gibert, F., Pascal, M.L., and Pichavant, M. (1998) Gold solubility and speciation in
663 hydrothermal solutions: Experimental study of the stability of hydrosulphide
664 complex of gold (AuHS degrees) at 350 to 450 degrees C and 500 bars. *Geochimica*
665 *Et Cosmochimica Acta*, 62(17), 2931-2947.
- 666 Guillong, M., and Heinrich, C.A. (2007) Sensitivity enhancement in laser ablation ICP-MS
667 using small amounts of hydrogen in the carrier gas. *Journal of Analytical Atomic*
668 *Spectrometry*, 22(12), 1488-1494.
- 669 Guillong, M., Meier, D., Allan, M., Heinrich, C., and Yardley, B. (2008) SILLS: a MATLAB-based
670 program for the reduction of laser ablation ICP-MS data of homogeneous materials
671 and inclusions. *Mineralogical Association of Canada Short Course*, 40, 328-333.
- 672 Günther, D., Audetat, A., Frischknecht, R., and Heinrich, C.A. (1998) Quantitative analysis of
673 major, minor and trace elements in fluid inclusions using laser ablation inductively

- 674 coupled plasma mass spectrometry. *Journal of Analytical Atomic Spectrometry*,
675 13(4), 263-270.
- 676 Hack, A.C., and Mavrogenes, J.A. (2006) A synthetic fluid inclusion study of copper solubility
677 in hydrothermal brines from 525 to 725 degrees C and 0.3 to 1.7 GPa. *Geochimica Et*
678 *Cosmochimica Acta*, 70(15), 3970-3985.
- 679 Hanley, J.J., Pettke, T., Mungall, J.E., and Spooner, E.T.C. (2005) The solubility of platinum
680 and gold in NaCl brines at 1.5 kbar, 600 to 800 degrees C: A laser ablation ICP-MS
681 pilot study of synthetic fluid inclusions (vol 10, pg 2593, 2005). *Geochimica Et*
682 *Cosmochimica Acta*, 69(23), 5635-5637.
- 683 Heinrich, C., Günther, D., Audétat, A., Ulrich, T., and Frischknecht, R. (1999) Metal
684 fractionation between magmatic brine and vapor, determined by microanalysis of
685 fluid inclusions. *Geology*, 27(8), 755-758.
- 686 Jochum, K.P., Nohl, L., Herwig, K., Lammel, E., Toll, B., and Hofmann, A.W. (2005) GeoReM: A
687 new geochemical database for reference materials and isotopic standards.
688 *Geostandards and Geoanalytical Research*, 29(3), 333-338.
- 689 Lerchbaumer, L., and Audetat, A. (2009) Partitioning of Cu between vapor and brine - An
690 experimental study based on LA-ICP-MS analysis of synthetic fluid inclusions.
691 *Geochimica Et Cosmochimica Acta*, 73(13), A744-A744.
- 692 Li, Y., and Audetat, A. (2009) A method to synthesize large fluid inclusions in quartz at
693 controlled times and under unfavorable growth conditions. *American Mineralogist*,
694 94(2-3), 367-371.
- 695 Loucks, R.R., and Mavrogenes, J.A. (1999) Gold solubility in supercritical hydrothermal
696 brines measured in synthetic fluid inclusions. *Science*, 284(5423), 2159-2163.
- 697 Matthews, W., Linnen, R.L., and Guo, Q. (2003) A filler-rod technique for controlling redox
698 conditions in cold-seal pressure vessels. *American Mineralogist*, 88(4), 701-707.
- 699 Newton, R.C., and Manning, C.E. (2000) Quartz solubility in H₂O-NaCl and H₂O-CO₂
700 solutions at deep crust-upper mantle pressures and temperatures: 2-15 kbar and
701 500-900 degrees C. *Geochimica Et Cosmochimica Acta*, 64(17), 2993-3005.
- 702 Pokrovski, G.S., Kokh, M.A., Guillaume, D., Borisova, A.Y., Gisquet, P., Hazemann, J.L., Lahera,
703 E., Del Net, W., Proux, O., Testemale, D., Haigis, V., Jonchiere, R., Seitsonen, A.P., Ferlat,
704 G., Vuilleumier, R., Saitta, A.M., Boiron, M.C., and Dubessy, J. (2015) Sulfur radical
705 species form gold deposits on Earth. *Proceedings of the National Academy of*
706 *Sciences of the United States of America*, 112(44), 13484-13489.
- 707 Roedder, E., and Kopp, O.C. (1975) A check on the validity of the pressure correction in
708 inclusion geothermometry, using hydrothermally grown quartz. *Fortschr. Miner.*, 52,
709 431-446.
- 710 Seo, J.H., Guillong, M., Aerts, M., Zajacz, Z., and Heinrich, C.A. (2011) Microanalysis of S, Cl,
711 and Br in fluid inclusions by LA-ICP-MS. *Chemical Geology*, 284(1-2), 35-44.
- 712 Seyfried, W.E., Gordon, P.C., and Dickson, F.W. (1979) New Reaction Cell for Hydrothermal
713 Solution Equipment. *American Mineralogist*, 64(5-6), 646-649.
- 714 Shelton, K.L., and Orville, P.M. (1980) Formation of Synthetic Fluid Inclusions in Natural
715 Quartz. *American Mineralogist*, 65(11-1), 1233-1236.
- 716 Simon, A.C., Frank, M.R., Pettke, T., Candela, P.A., Piccoli, P.M., Heinrich, C.A., and Glascock,
717 M. (2007) An evaluation of synthetic fluid inclusions for the purpose of trapping
718 equilibrated, coexisting, immiscible fluid phases at magmatic conditions. *American*
719 *Mineralogist*, 92(1), 124-138.

- 720 Simon, A.C., Pettke, T., Candela, P.A., Piccolli, P.M., and Heinrich, C.A. (2006) Copper
721 partitioning in a melt-vapor-brine-magnetite-pyrrhotite assemblage. *Geochimica Et*
722 *Cosmochimica Acta*, 70(22), 5583-5600.
- 723 Sterner, S.M., and Bodnar, R.J. (1984) Synthetic Fluid Inclusions in Natural Quartz .1.
724 Compositional Types Synthesized and Applications to Experimental Geochemistry.
725 *Geochimica Et Cosmochimica Acta*, 48(12), 2659-2668.
- 726 Sterner, S.M., Hall, D.L., and Bodnar, R.J. (1988) Synthetic Fluid Inclusions. V. Solubility
727 Relations in the System NaCl-KCl-H₂O under Vapor-Saturated Conditions.
728 *Geochimica Et Cosmochimica Acta*, 52(5), 989-1005.
- 729 Ulrich, T., and Mavrogenes, J. (2008) An experimental study of the solubility of molybdenum
730 in H₂O and KCl-H₂O solutions from 500 degrees C to 800 degrees C, and 150 to 300
731 MPa. *Geochimica Et Cosmochimica Acta*, 72(9), 2316-2330.
- 732 Zajacz, Z., Seo, J.H., Candela, P.A., Piccoli, P.M., Heinrich, C.A., and Guillong, M. (2010) Alkali
733 metals control the release of gold from volatile-rich magmas. *Earth and Planetary*
734 *Science Letters*, 297(1-2), 50-56.
- 735 Zhang, L., Audetat, A., and Dolejs, D. (2012) Solubility of molybdenite (MoS₂) in aqueous
736 fluids at 600-800 degrees C, 200 MPa: A synthetic fluid inclusion study. *Geochimica*
737 *Et Cosmochimica Acta*, 77, 175-185.

738

739